星形成ゼミ
GAEP 2024/11/12-11/14
担当：小道 雄斗（東大相川研D1）

Water vapor as a probe of the origin of gas in debris disks

Yasuhiro Hasegawa[1], Riouhei Nakatani[1,2], Isabel Rebollido[3], Meredith MacGregor[4], Björn J. R. Davidsson[1], Dariusz C. Lis[1], Neal Turner[1], and Karen Willacy[1]

[1] Jet Propulsion Laboratory, California Institute of Technology, Pasadena, CA 91109, USA
e-mail: yasuhiro.hasegawa@jpl.nasa.gov
[2] RIKEN Cluster for Pioneering Research, 2-1 Hirosawa, Wako-shi, Saitama 351-0198, Japan
[3] European Space Agency (ESA), European Space Astronomy Centre (ESAC), Camino Bajo del Castillo s/n, 28692 Villanueva de la Cañada, Madrid, Spain
[4] Department of Physics and Astronomy, Johns Hopkins University, 3400 N Charles Street, Baltimore, MD 21218, USA

Received; accepted

ABSTRACT

Context. Debris disks embrace the formation and evolution histories of planetary systems. Recent detections of gas in these disks have received considerable attention, as its origin ties up ongoing disk evolution and the present composition of planet-forming materials.
Aims. Observations of the CO gas alone, however, cannot reliably differentiate between two leading, competing hypotheses: (1) the observed gas is the leftover of protoplanetary disk gas, and (2) the gas is the outcome of collisions between icy bodies. We propose that such differentiation may become possible by observing cold water vapor.
Methods. Order-of-magnitude analyses and comparison with existing observations are performed.
Results. We show that different hypotheses lead to different masses of water vapor. This occurs because, for both hypotheses, the presence of cold water vapor is attributed to photodesorption from dust particles by attenuated interstellar UV radiation. Cold water vapor cannot be observed by current astronomical facilities as most of its emission lines fall in the far-IR (FIR) range.
Conclusions. This work highlights the need for a future FIR space observatory to reveal the origin of gas in debris disks and the evolution of planet-forming disks in general.

Key words. astrochemistry – accretion, accretion disks – protoplanetary disks – comets: general – circumstellar matter

デブリ円盤中のガスの起源について、オーダー計算で調べた論文

イントロ

- デブリ円盤中のガスの検出(e.g. Dent+14, Kral+17)

  原子: C, O, Na, … 分子: CO

- 円盤中のガスの起源: 2つの仮説

1. 原始惑星系円盤時代のガスの名残(hypothesis 1; primordial origin)
2. 円盤中のガスが散逸した後、微惑星衝突により供給 (hypothesis 2; secondary origin)

   どちらが優勢かは現在も議論が続いている

- COと(冷たい)水蒸気に注目

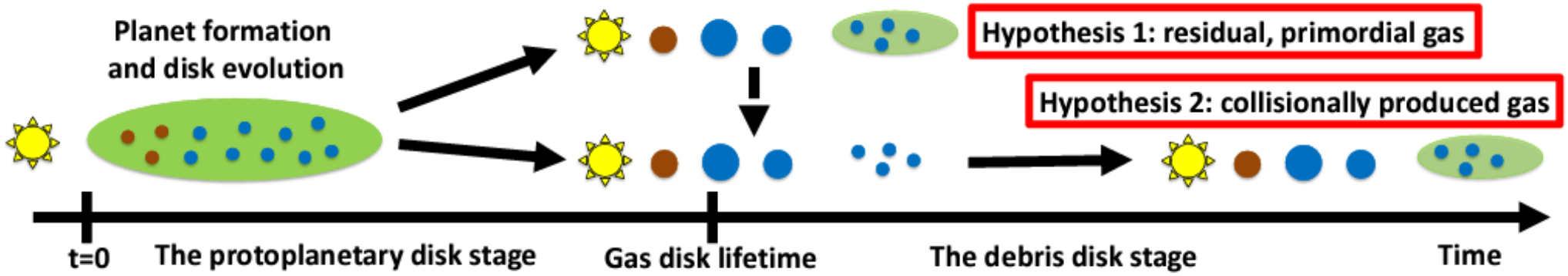

Fig. 1. A schematic diagram of time-evolution of planet-forming disks. The host star is denoted by the star symbol, planet-forming materials are represented by the brown and blue dots, and disk gas by the green ovals. Hypothesis 1 considers that observed gas is the leftover of primordial gas, while Hypothesis 2 considers that the gas is produced by collisions among icy bodies.

CO質量の評価

- COの総質量

典型的な光蒸発率: $\sim 10^{-10}\ M_\odot\ \mathrm{yr}^{-1}$, 遷移円盤の時間スケール: $10^5\ \mathrm{yr}$

→ 遷移円盤のガス総質量: $1\ M_\oplus$

ガス全体に対するCO質量の割合: $f_{\mathrm{CO,gas}} \equiv \frac{M_{\mathrm{CO,gas}}}{M_{\mathrm{gas}}} \simeq \frac{M_{\mathrm{CO,gas}}}{M_{\mathrm{H_2}}} = \frac{m_{\mathrm{CO}} N_{\mathrm{CO}}}{m_{\mathrm{H_2}} N_{\mathrm{H_2}}} \sim 10^{-3}$
(相対存在度: 10^{-4} より)

→ 遷移円盤のCO総質量: $10^{-3}\ M_\oplus$

CO質量がこれよりも多いとprimordial, 少ないとsecondary

- COガスとダスト質量の比(primordialの場合)

観測されるCOの量は気相中の存在度(気相化学反応)で決まる

$$\left.\frac{\overline{M}_{\mathrm{CO}}}{\overline{M}_{\mathrm{solid}}}\right|_{\mathrm{Hyp1}} \simeq \frac{M_{\mathrm{CO,gas}}}{M_{\mathrm{solid}}} = \frac{M_{\mathrm{CO,gas}}}{M_{\mathrm{gas}}} \frac{M_{\mathrm{gas}}}{M_{\mathrm{solid}}} \simeq f_{\mathrm{CO,gas}} f_{\mathrm{GtoS}}, \qquad f_{\mathrm{GtoS}} \equiv \frac{M_{\mathrm{gas}}}{M_{\mathrm{solid}}} \sim 10^2$$

$$\left.\frac{\overline{M}_{\mathrm{CO}}}{\overline{M}_{\mathrm{solid}}}\right|_{\mathrm{Hyp1}} \simeq 10^{-1} \left(\frac{f_{\mathrm{CO,gas}}}{10^{-3}}\right)\left(\frac{f_{\mathrm{GtoS}}}{10^2}\right)$$

CO質量の評価

- COガスとダスト質量の比(secondaryの場合)

観測されるCOの量はダスト表面のCO氷の量を反映していると考える

氷と岩石の質量比(彗星やKuiper Belt天体より引用)

$$f_{\rm ItoR} \equiv \frac{M_{\rm Z,ice}}{M_{\rm Z,ref}} \sim 0.1$$

COガスとダストの質量比
(氷の主成分は水氷、彗星でのCOと水氷の存在量比10%を仮定)

$$\left.\frac{\overline{M}_{\rm CO}}{\overline{M}_{\rm solid}}\right|_{\rm Hyp2} \simeq \frac{M_{\rm CO,ice}}{M_{\rm Z,ref}} = \frac{M_{\rm CO,ice}}{M_{\rm Z,ice}}\frac{M_{\rm Z,ice}}{M_{\rm Z,ref}} \simeq f_{\rm CO,ice} f_{\rm ItoR}$$

$$f_{\rm CO,ice} \equiv \frac{M_{\rm CO,ice}}{M_{\rm Z,ice}} \simeq \frac{M_{\rm CO,ice}}{M_{\rm H_2O,ice}} \simeq \frac{m_{\rm CO} N_{\rm CO,ice}}{m_{\rm H_2O} N_{\rm H_2O,ice}} \sim 10^{-1}$$

$$\left.\frac{\overline{M}_{\rm CO}}{\overline{M}_{\rm solid}}\right|_{\rm Hyp2} \simeq 10^{-2}\left(\frac{f_{\rm CO,ice}}{10^{-1}}\right)\left(\frac{f_{\rm ItoR}}{10^{-1}}\right)$$

観測との比較

パラメータ範囲は以下の表を採用

primordialはCOガスに富んだ円盤を、
secondaryはCOガスに乏しい円盤を再現

双方の仮説で同程度のCO/solid質量比を
示唆しており、仮説の区別は困難
(CO質量が単調減少するとも限らない)

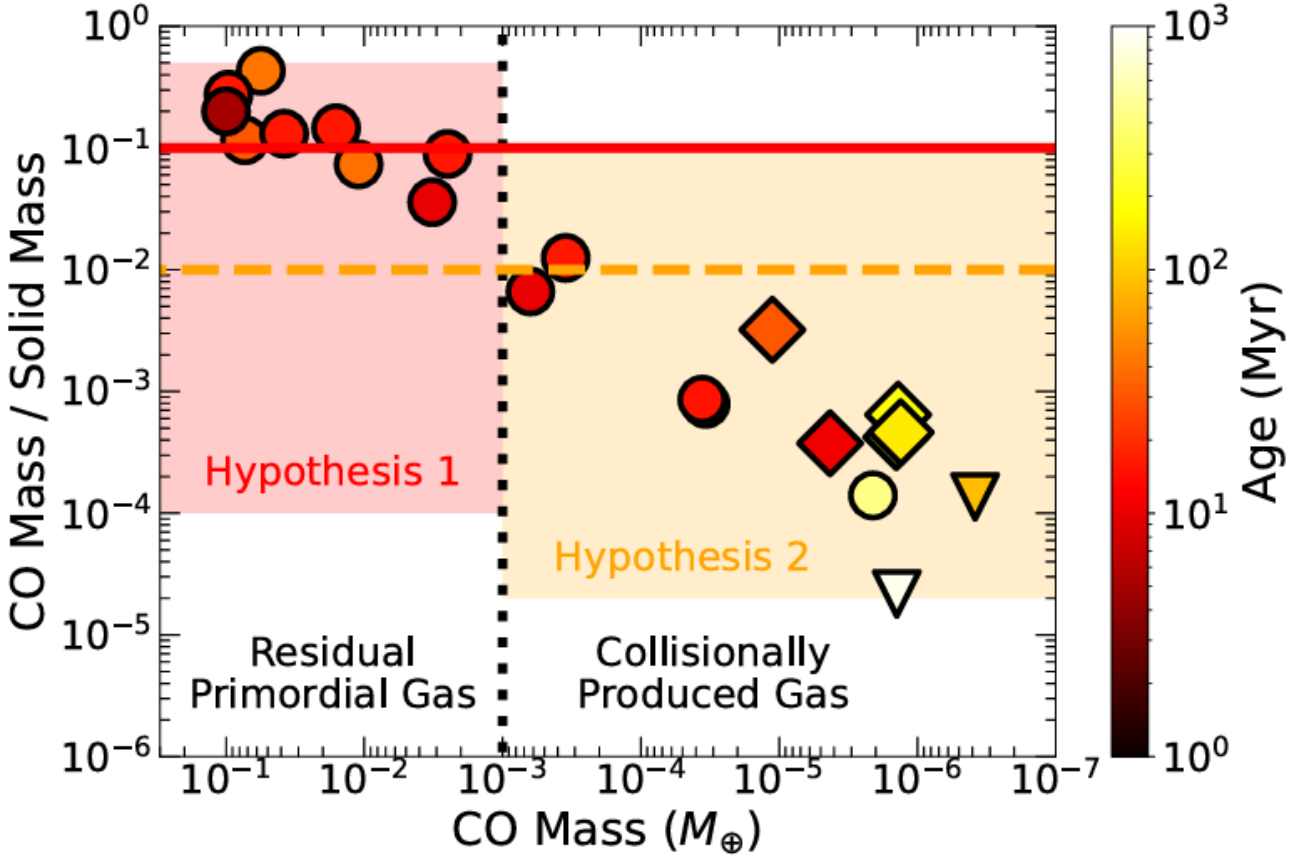

Hypothesis	Possible ranges	Resulting values	Reference
Hypothesis 1	$10^{-4} \lesssim f_{\mathrm{CO,gas}} \lesssim 10^{-3}$ $1 \lesssim f_{\mathrm{GtoS}} \lesssim 5 \times 10^{2}$	$10^{-4} \lesssim M_{\mathrm{CO}}/M_{\mathrm{solid}} \lesssim 0.5$ $2 \times 10^{-6} \lesssim M_{\mathrm{H_2O}}/M_{\mathrm{CO}} \lesssim 10^{-2}$	(1)
Hypothesis 2	$4 \times 10^{-3} \lesssim f_{\mathrm{CO,ice}} \lesssim 0.3$ $5 \times 10^{-3} \lesssim f_{\mathrm{ItoR}} \lesssim 0.3$	$2 \times 10^{-5} \lesssim M_{\mathrm{CO}}/M_{\mathrm{Solid}} \lesssim 9 \times 10^{-2}$ $10^{-4} \lesssim M_{\mathrm{H_2O}}/M_{\mathrm{CO}} \lesssim 0.5$	(2)

(1) The range of $f_{\mathrm{CO,gas}}$ comes from Bolatto et al. (2013); Favre et al. (2013); France et al. (2014); Cauley et al. (2021), while that of f_{GtoS} is from Miotello et al. (2017).

(2) The range of $f_{\mathrm{CO,ice}}$ is motivated by Mumma & Charnley (2011); Harrington Pinto et al. (2022), while that of f_{ItoR} is by Fulle et al. (2019); Choukroun et al. (2020).

水蒸気質量の評価

- 冷たい水蒸気

円盤のうちUVが程々に透過している場所では、光脱離により水蒸気が存在する

水蒸気の存在量は光脱離率と光解離率のつり合いで決まる
(Y: photodesorption yield, $N_{\rm dust}$: photodesorptionに寄与するダストの存在度)

$$\sigma_{\rm photo} N_{\rm H_2O,vap} = \sigma_{\rm dust} Y N_{\rm dust}$$

- Primordial origin

$f_{\rm dust} = 10^{-2}$: 光蒸発に効くダスト(サイズ0.1 μmのダスト)の割合

$$N_{\rm dust} \equiv f_{\rm dust} M_{\rm solid} / m_{\rm dust}$$

$$\frac{N_{\rm H_2O,vap}}{N_{\rm H_2}} = Y \frac{\sigma_{\rm dust}}{\sigma_{\rm photo}} \frac{N_{\rm dust}}{N_{\rm H_2}} \sim 10^{-9} \left(\frac{f_{\rm GtoS}}{10^2}\right)^{-1} \left(\frac{r_{\rm dust}}{0.1\ \mu{\rm m}}\right)^{-1}$$

$$\left.\frac{\overline{M}_{\rm H_2O}}{\overline{M}_{\rm CO}}\right|_{\rm Hyp1} \simeq \frac{m_{\rm H_2O} N_{\rm H_2O,vap}}{M_{\rm CO,gas}} = \frac{M_{\rm H_2}}{M_{\rm CO,gas}} \frac{m_{\rm H_2O} N_{\rm H_2O,vap}}{m_{\rm H_2} N_{\rm H_2}}$$

$$\sim 10^{-5} \left(\frac{f_{\rm CO,gas}}{10^{-3}}\right)^{-1} \left(\frac{f_{\rm GtoS}}{10^2}\right)^{-1} \left(\frac{r_{\rm dust}}{0.1\mu{\rm m}}\right)^{-1}.$$

水蒸気質量の評価

- Secondary origin

$$N_{\rm dust} \equiv f_{\rm dust} M_{\rm Z,ref} / m_{\rm dust}$$

$$N_{\rm H_2O,ice} \simeq M_{\rm Z,ice} / m_{\rm H_2O}$$

$$\frac{N_{\rm H_2O,vap}}{N_{\rm H_2O,ice}} = Y \frac{\sigma_{\rm dust}}{\sigma_{\rm photo}} \frac{N_{\rm dust}}{N_{\rm H_2O,ice}} \sim 10^{-4} \left(\frac{f_{\rm ItoR}}{10^{-1}} \right)^{-1} \left(\frac{r_{\rm dust}}{1\,\mu{\rm m}} \right)^{-1}$$

$f_{\rm dust} = 1$: 光蒸発に効くダスト(サイズ1 μmのダスト)の割合
... 観測される質量比は氷組成を反映していると仮定し、1と設定

$$\left. \frac{\overline{M}_{\rm H_2O}}{\overline{M}_{\rm CO}} \right|_{\rm Hyp2} \simeq \frac{m_{\rm H_2O} N_{\rm H_2O,vap}}{M_{\rm CO,ice}} = \frac{M_{\rm H_2O,ice}}{M_{\rm CO,ice}} \frac{N_{\rm H_2O,vap}}{N_{\rm H_2O,ice}}$$

$$\sim 10^{-3} \left(\frac{f_{\rm CO,ice}}{10^{-1}} \right)^{-1} \left(\frac{f_{\rm ItoR}}{10^{-1}} \right)^{-1} \left(\frac{r_{\rm dust}}{1\,\mu{\rm m}} \right)^{-1}$$

水蒸気の観測の推定値

H_2O質量とH_2O/solid比にはjumpが見られるはず
Monte-Carlo推定でも各パラメータの範囲内でjumpは見えるはず

→ primordialかsecondaryかを区別するCO質量の観測的推定が可能になるはず

HerschelによるTW Hyaでの水蒸気の観測や、β Picでの上限値と整合的

将来観測に期待

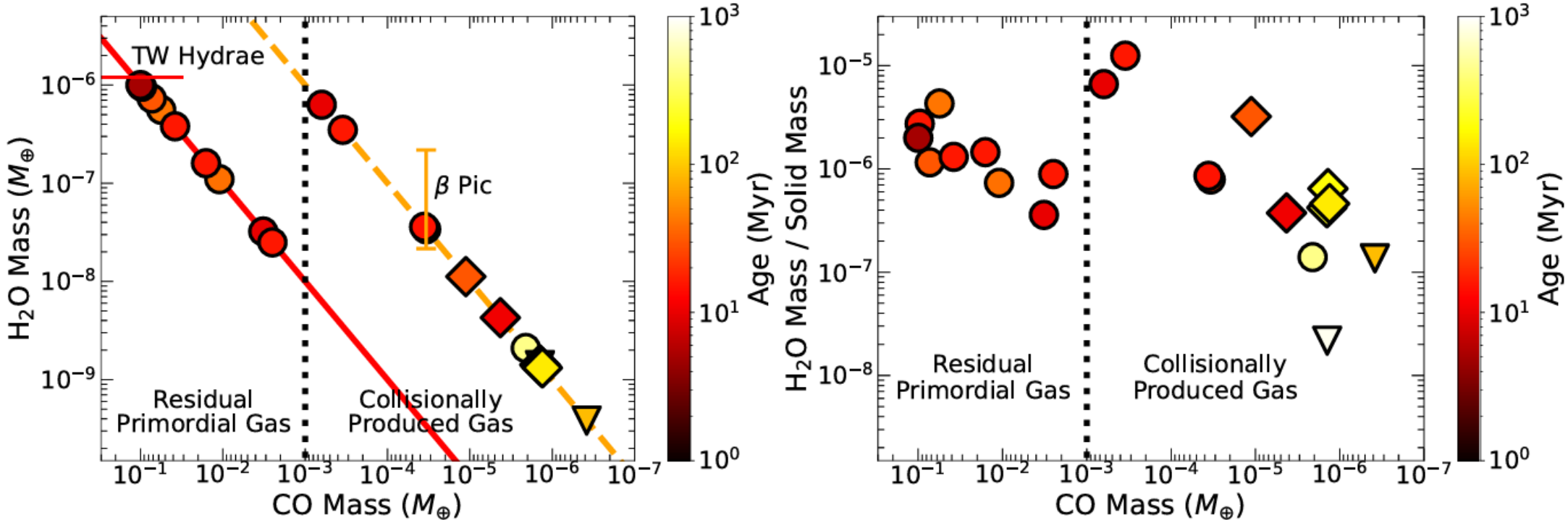

Revisiting rotationally excited CH at radio wavelengths: A case study towards W51

Arshia M. Jacob[1,2], Meera Nandakumar[3], Nirupam Roy[3], Karl M. Menten[2], David A. Neufeld[1], Alexandre Faure[4], Maitraiyee Tiwari[2], Thushara G. S. Pillai[5,6], Timothy Robishaw[7], and Carlos A. Durán[8]

ABSTRACT

Context. Ever since they were first detected in the interstellar medium, the radio wavelength (3.3 GHz) hyperfine-structure splitting transitions in the rotational ground state of CH have been observed to show anomalous excitation. Astonishingly, this behaviour has been uniformly observed towards a variety of different sources probing a wide range of physical conditions. While the observed level inversion can be explained globally by a pumping scheme involving collisions, a description of the extent of 'over-excitation' observed in individual sources requires the inclusion of radiative processes, involving transitions at higher rotational levels. Therefore, a complete description of the excitation mechanism in the CH ground state, observed towards individual sources entails observational constraints from the rotationally excited levels of CH and in particular that of its first rotationally excited state ($^2\Pi_{3/2}, N = 1, J = 3/2$).
Aims. Given the limited detections of these lines, the objective of this work is to characterise the physical and excitation properties of the rotationally excited lines of CH between the Λ-doublet levels of its $^2\Pi_{3/2}, N = 1, J = 3/2$ state near 700 MHz, and investigate their influence on the pumping mechanisms of the ground-state lines of CH.
Methods. This work presents the first interferometric search for the rotationally excited lines of CH between the Λ-doublet levels of its $^2\Pi_{3/2}, N = 1, J = 3/2$ state near 700 MHz carried out using the upgraded Giant Metrewave Radio Telescope (uGMRT) array towards six star-forming regions, W51 E, Sgr B2 (M), M8, M17, W43 and DR21 Main.
Results. We detect the two main hyperfine structure lines within the first rotationally excited state of CH, in absorption towards W51 E. To jointly model the physical and excitation conditions traced by lines from both the ground and first rotationally excited states of CH, we performed non-local thermodynamic equilibrium (LTE) radiative transfer calculations using the code MOLPOP-CEP. These models account for the effects of line overlap and are aided by column density constraints from the far-infrared (FIR) wavelength rotational transitions of CH that connect to the ground state and use collisional rate coefficients for collisions of CH with H, H_2 and electrons (the latter are computed in this work using cross-sections estimated within the Born approximation).
Conclusions. The non-LTE analysis revealed that physical properties typical of diffuse and translucent clouds best reproduce the higher rates of level inversion seen in the ground-state lines at 3.3 GHz, observed at velocities near 66 km s^{-1} along the sightline towards W51 E. In contrast, the excited lines near 700 MHz were only excited in much denser environments with $n_H \sim 10^5$ cm^{-3} towards which the anomalous excitation in two of the three ground state lines is quenched, but not in the 3.264 GHz line. This is in alignment with our observations and suggests that while FIR pumping and line overlap effects are essential for exciting and producing line inversion in the ground state, excitation to the first rotational level is dominated by collisional excitation from the ground state. For the rotationally excited state of CH, the models indicate low excitation temperatures and column densities of 2×10^{14} cm^{-2}. Furthermore, modelling these lines helps us understand the complexities of the spectral features observed in the 532/536 GHz rotational transitions of CH. These transitions, connecting sub-levels of the first rotationally excited state to the ground state, play a crucial role in trapping FIR radiation and enhancing the degree of inversion seen in the ground state lines. Based on the physical conditions constrained, we predict the potential of detecting hyperfine-splitting transitions arising from higher rotationally excited transitions of CH in the context of their current non-detections.

W51を始めとした天体についてCHを観測し、励起状態について考察した論文

イントロ

- CHの励起状態は複雑

基底状態から衝突によりJ=3/2へ励起

衝突励起時、パリティは + → + の方が - → - よりも起こりやすいため、
J=3/2のうち低エネルギー側に貯まる

→ J=3/2からは即座にJ=1/2の – へ
　脱励起するため、
　J=1/2でover-populationが起こる

→ maserとして振る舞う

遠赤外線の外部輻射による
励起もpumpingに重要

CHの励起状態の理解のために、
さらに700 MHzの遷移についても
調べる

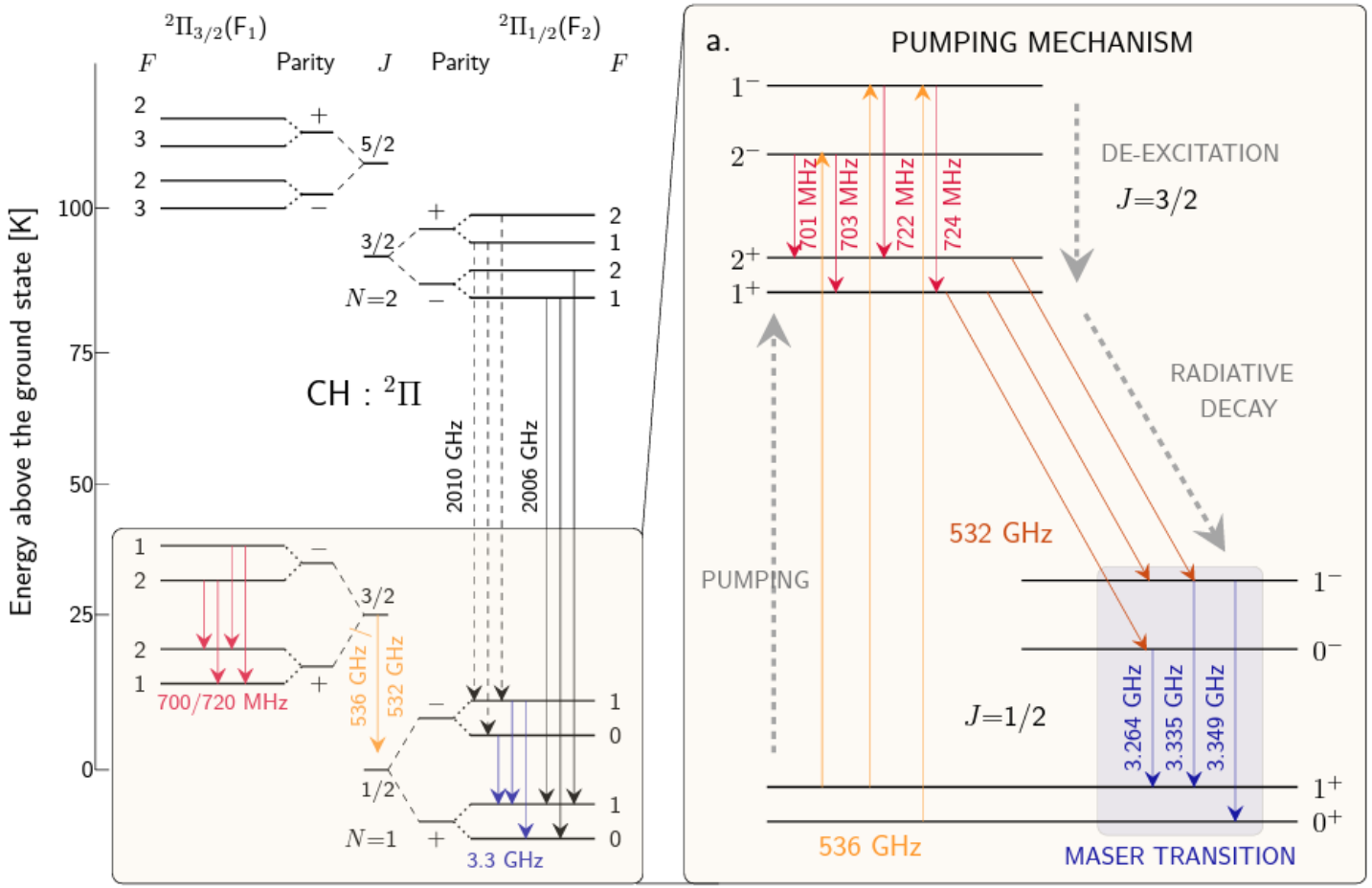

観測・結果

右表の星形成領域を対象

Giant Metrewave Radio Telescopeを使用

Source	Coordinates (J2000)		d	v_{LSR}	Frequency	$\theta_{maj} \times \theta_{min}$	P.A.	rms	$S_{cont,peak}$
	α [hh:mm:ss]	δ [dd:mm:ss]	[kpc]	[km s^{-1}]	[GHz]	[″ × ″]	[°]	[mJy/beam]	[Jy]
Sgr B2 (M)	17:47:20.50	−28:23:06.00	8.2	64.0	701	27.6 × 27.4	71.4	5.8	0.69
					703	25.7 × 22.5	−2.8	4.2	0.67
					722	30.2 × 25.0	6.2	5.7	0.70
					724	32.3 × 26.8	−6.4	6.4	0.81
M8	18:03:37.00	−24:23:12.00	1.3	10.0	701	38.0 × 22.6	18.0	26.4	1.80
					703	33.7 × 22.8	23.8	25.7	1.81
					722	41.2 × 26.5	18.0	21.8	1.64
					724	43.6 × 27.9	14.5	21.9	1.65
M17	18:20:47.00	−16:10:18.00	1.8	22.0	701	46.6 × 40.2	36.2	9.3	2.60
					703	28.7 × 21.4	32.6	16.3	2.44
					722	33.8 × 23.9	33.1	17.2	2.31
					724	33.4 × 24.4	33.3	13.3	2.39
W43	18:47:32.40	−01:56:31.00	3.1	97.8	701	20.8 × 15.2	43.7	2.0	1.44
					703	25.5 × 18.2	57.1	0.8	1.85
					722	33.1 × 21.2	50.5	1.2	1.79
					724	31.6 × 22.1	44.2	2.5	1.40
W51 E	19:23:43.90	+14:30:31.00	5.4	57.0	701	35.5 × 26.2	33.2	8.4	3.11
					703	35.5 × 30.1	27.0	4.7	2.34
					722	38.6 × 26.9	39.8	6.8	3.06
					724	42.1 × 31.2	32.9	24.9	2.36
DR21 Main	20:39:01.59	+42:19:37.80	1.5	−4.0	701	10.2 × 6.4	36.2	2.4	2.33
					703	13.9 × 8.4	44.4	2.1	2.16
					722	13.9 × 8.3	44.4	1.6	2.23
					724	10.2 × 6.5	43.5	4.4	2.39

Frequency [MHz]	v_{LSR} [km s^{-1}]	Δv [km s^{-1}]	Peak T_B [K]	$\int T_B \Delta v$ [K km s^{-1}]
3264	51.6 ± 3.1	5.7 ± 0.3	1.8 ± 0.1	10.1 ± 0.8
	56.1 ± 3.2	3.8 ± 0.2	12.0 ± 0.7	45.6 ± 3.6
	61.3 ± 2.6	5.0 ± 0.2	0.8 ± 0.03	4.1 ± 0.2
	65.3 ± 3.2	2.5 ± 0.1	28.4 ± 1.5	71.0 ± 4.7
	67.0 ± 2.4	4.1 ± 0.2	7.0 ± 0.3	28.7 ± 1.8
3335	51.7 ± 3.0	5.7 ± 0.3	−1.6 ± 0.1	−9.1 ± 0.7
	56.1 ± 3.2	3.9 ± 0.2	−2.5 ± 0.1	−9.8 ± 0.6
	61.3 ± 3.6	5.0 ± 0.3	−3.3 ± 0.2	−16.5 ± 1.4
	65.3 ± 2.7	2.5 ± 0.1	−6.0 ± 0.3	−15.0 ± 1.0
	67.0 ± 3.0	4.1 ± 0.2	5.0 ± 0.2	20.5 ± 1.3
3349	51.6 ± 3.0	5.6 ± 0.3	−0.07 ± 0.01	−0.4 ± 0.06
	56.1 ± 3.2	3.9 ± 0.2	−1.4 ± 0.1	−5.5 ± 0.5
	61.3 ± 3.5	5.0 ± 0.3	−0.8 ± 0.04	−3.8 ± 0.3
	65.3 ± 3.6	2.5 ± 0.2	3.9 ± 0.2	9.8 ± 1.0
	67.0 ± 3.3	4.1 ± 0.2	2.5 ± 0.1	10.3 ± 0.6
701	51.5 ± 6.5	5.7 ± 0.7	−47.7 ± 5.8	−267.1 ± 47.0
	56.2 ± 6.3	3.9 ± 0.5	−22.0 ± 2.5	−85.8 ± 14.7
	61.4 ± 7.1	5.0 ± 0.6	−20.2 ± 2.2	−101.0 ± 16.3
724	51.7 ± 8.0	5.7 ± 0.8	−28.5 ± 4.0	162.5 ± 32.2
	56.3 ± 7.2	3.9 ± 0.5	−15.0 ± 2.0	−58.5 ± 10.8
	61.4 ± 8.0	5.0 ± 0.7	−17.0 ± 2.2	−85.0 ± 16.0

- W51 Eのみで701, 724 MHzでのCH吸収線を観測
- Multiple Gaussian fittingを実行(左表)
  700 MHz線は3.3GHz線のうち低速度側のcloudをトレース
- non-LTE fittingを実行

結果

- non-LTE fitting

700 MHzで見えなかった速度成分は
比較的低密度かつ高温

700 MHzで見えている成分は
比較的高密度

→ 700 MHzは高密度での
衝突励起が重要

灰色: R_3
青色: 励起したCHの柱密度

$$R_1 = T_{3.264\ \mathrm{GHz}}/T_{3.349\ \mathrm{GHz}}$$
$$R_2 = T_{3.335\ \mathrm{GHz}}/T_{3.349\ \mathrm{GHz}}$$
$$R_3 = T_{701\ \mathrm{MHz}}/T_{724\ \mathrm{MHz}}$$

Velocity component [km s^{-1}]	$\lvert R_i \rvert$	$\log_{10}(n_{\mathrm{H}}/[\mathrm{cm}^{-3}])$	T_{kin} [K]
51	25.2	$5.32^{+0.18}_{-0.44}$	$63^{+10.0}_{-12.0}$
	22.8		
	1.8		
57	8.6	$5.02^{+0.26}_{-0.20}$	$72^{+8.0}_{-19.0}$
	1.8		
	1.5		
61	1.0	$5.3^{+0.10}_{-0.14}$	$27^{+4.0}_{-5.0}$
	4.1		
	1.2		
65	7.3	$3.25^{+0.08}_{-0.12}$	≥ 178
	1.5		
	–		
67	2.8	$2.49^{+0.22}_{-0.17}$	≥ 172
	1.6		
	–		

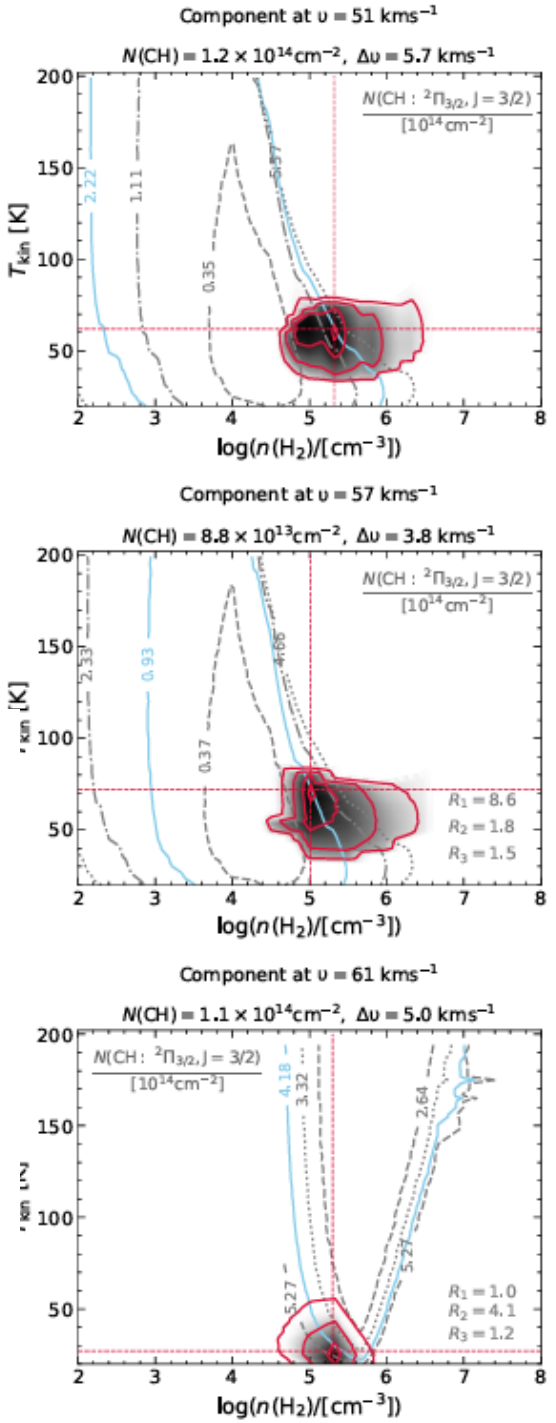

結果

- 励起曲線
  - 3.3 GHzの励起温度は概ね負

低密度の成分では
外部輻射によるpumping

高密度では衝突励起が効いている

高密度($\gtrsim 10^6$ cm^{-3})で正となる

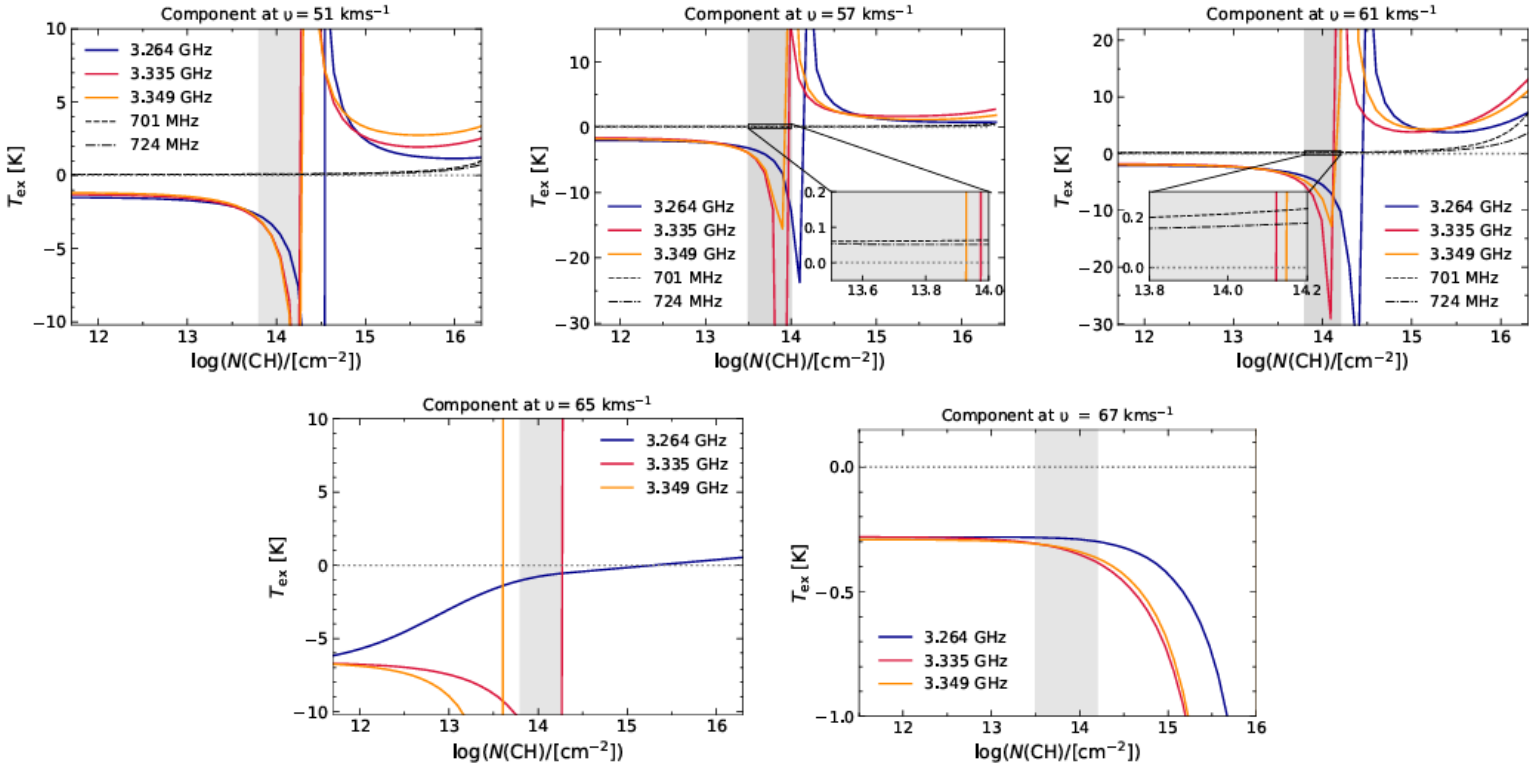

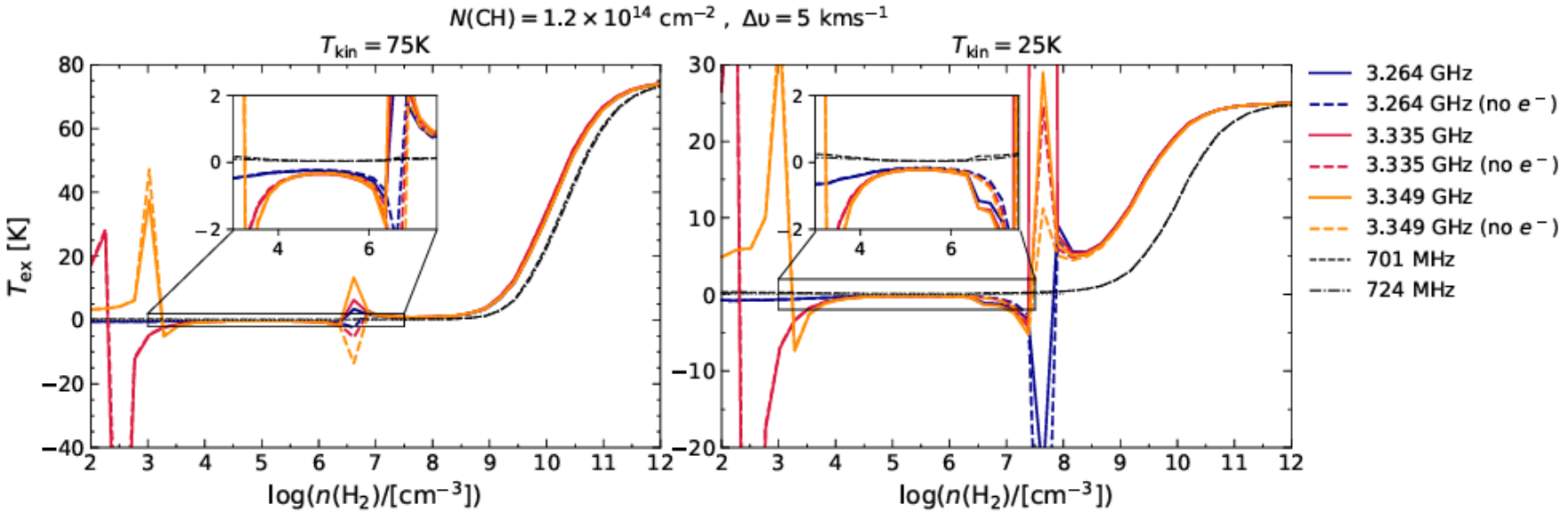

- 700 MHzの励起温度は
  Tex < 2 K

thermalizedするのは
およそ$\gtrsim 10^8$ cm^{-3}

結果

- 励起曲線
  - 3.3 GHzの励起温度は概ね負

低密度の成分では
外部輻射によるpumping

高密度では衝突励起が効いている

高密度($\gtrsim 10^6$ cm^{-3})で正となる

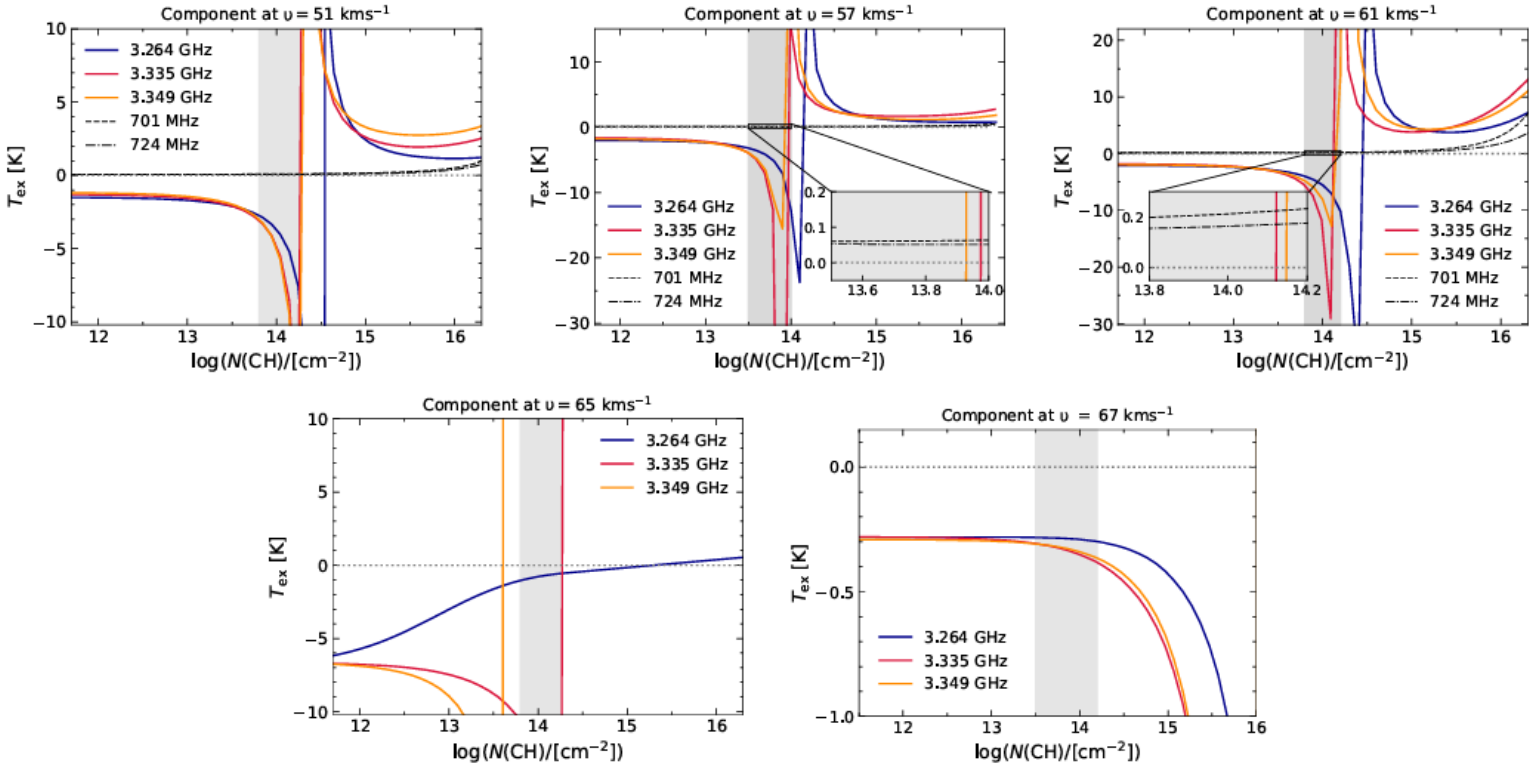

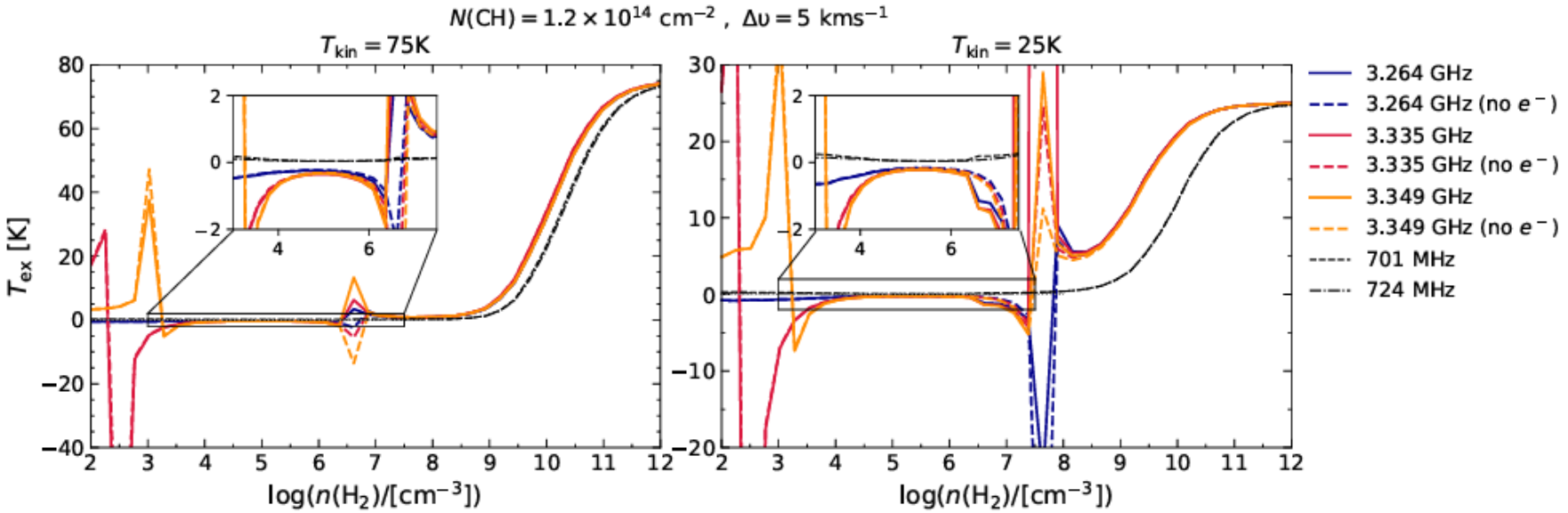

- 700 MHzの励起温度は
  Tex < 2 K

thermalizedするのは
およそ$\gtrsim 10^8$ cm^{-3}

- 532/536 GHzの理解に
今後役立つと思われる

ALMA Survey of Orion Planck Galactic Cold Clumps (ALMASOP): Nested Morphological and Kinematic Structures of Outflows Revealed in SiO and CO Emission

Chun-Fan Liu (劉君帆) [1], Hsien Shang (尚賢) [1], Doug Johnstone [2,3], Tsung-Han Ai (艾宗瀚) [1,4], Tsz Ming Lee (李子銘) [1,5], Ruben Krasnopolsky [1], Naomi Hirano [1], Somnath Dutta [1], Shih-Ying Hsu (許世穎) [1], Jesús Alejandro López-Vázquez [1], Sheng-Yuan Liu (呂聖元) [1], Tie Liu [6], Ken'ichi Tatematsu [7,8], Qizhou Zhang [9], Mark G. Rawlings [10], David Eden [11], Zhiyuan Ren [12], Patricio Sanhueza [13,14], Woojin Kwon [15,16], Chang Won Lee [17,18], Yi-Jehng Kuan (管一政) [1,19], Somdeb Bandopadhyay [1], Miikka S. Väisälä [1], Chin-Fei Lee (李景輝) [1], and Indrani Das [1]

The Atacama Large Millimeter/submillimeter Array Survey of Orion Planck Galactic Cold Clumps (ALMASOP) reveals complex nested morphological and kinematic features of molecular outflows through the CO ($J = 2-1$) and SiO ($J = 5-4$) emission. We characterize the jet and outflow kinematics of the ALMASOP sample in four representative sources (HOPS 10, 315, 358, and G203.21-11.20W2) through channel maps and position–velocity diagrams (PVDs) parallel and transverse to the outflow axes. The combined CO and SiO emission exhibits the coexistence of the conventional extremely–high-velocity (EHV) jets and shell-like low-velocity (LV) cavity walls and new features. More complex, nested bubble-like and filamentary structures in the images and channel maps, triangle-shaped regions near the base of the parallel PVDs, and regions composed of rhombus/oval shapes in the transverse PVDs, are also evident. Such features find natural explanations within the bubble structure of the unified model of jet, wind, and ambient medium. The reverse shock cavity is revealed on the PVD base regions, and other features naturally arise within the dynamic postshock region of magnetic interaction. The finer nested shells observed within the compressed wind region reveal previously unnoticed shocked emission between the jet and the conventional large cavity walls. These pseudopulse-produced filamentary features connect to the jet-like knotty blobs, creating an impression of episodicity in mass ejection. SiO emission is enhanced downstream of the reverse shock boundary, with jet-like excitation conditions. Combined, these observed features reveal the extended structures induced by the magnetic interplay between a jet-bearing magnetized wide-angle wind and its ambient magnetized surrounding medium.

ALMAによる outflowの観測

Source Name	HOPS ID	RA (J2000)	Dec (J2000)	PA_{red} (°)	i (°)	v_{sys} ($km\,s^{-1}$)	Protostellar Class
(1)	(2)	(3)	(4)	(5)	(6)	(7)	(8)
G205.46-14.56S3	315	05h46m03.63s	-00d14m49.57s	227.3	40°	10 ± 2	I
G209.55-19.68S2	10	05h35m09.05s	-05d58m26.87s	33.6	62°	8 ± 2	0
G203.21-11.20W2	···	05h53m39.51s	+03d22m23.85s	149.1	72°	10 ± 2	0
G205.46-14.56S1_A	358	05h46m07.26s	-00d13m30.23s	163.4	89°	10 ± 2	0

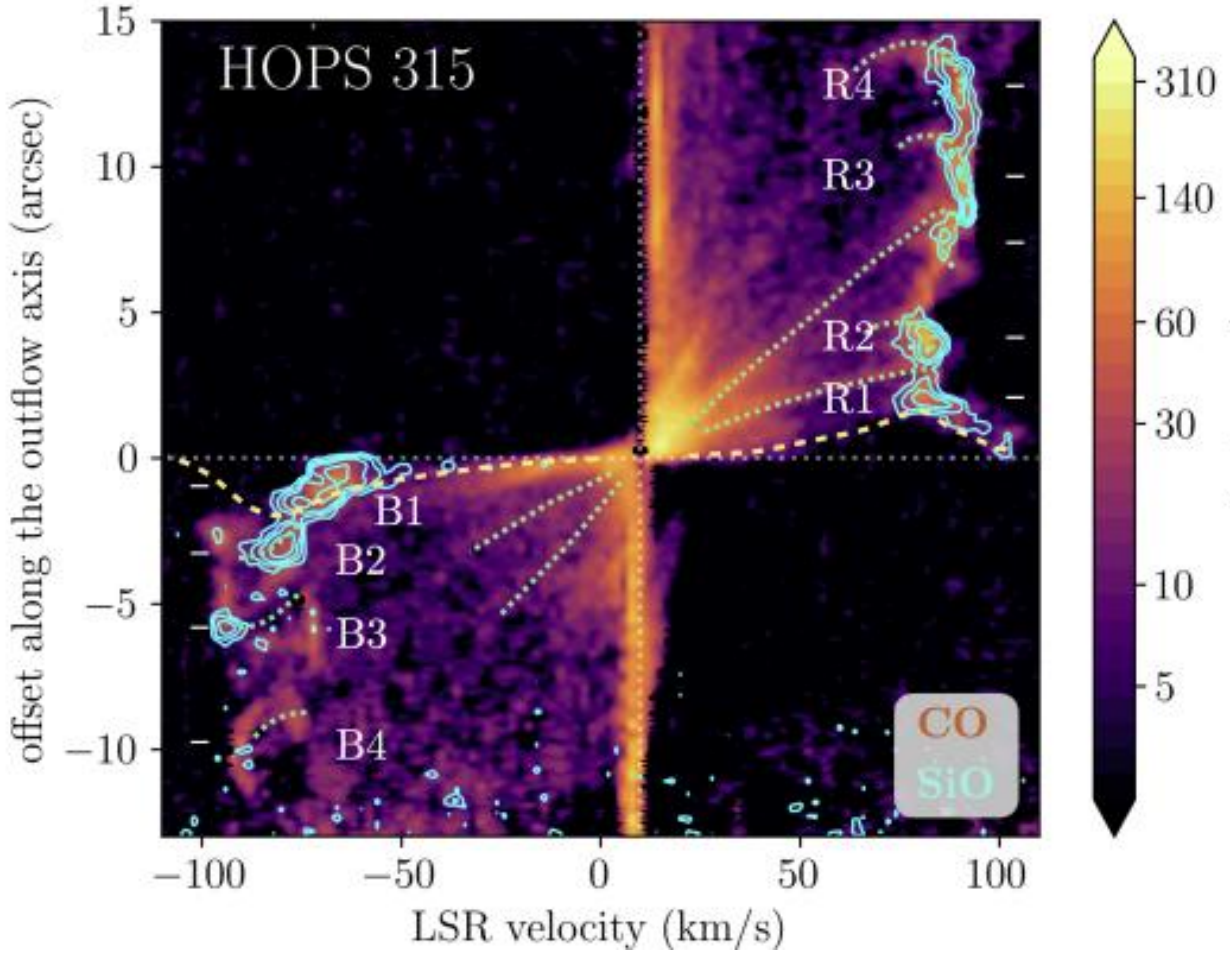

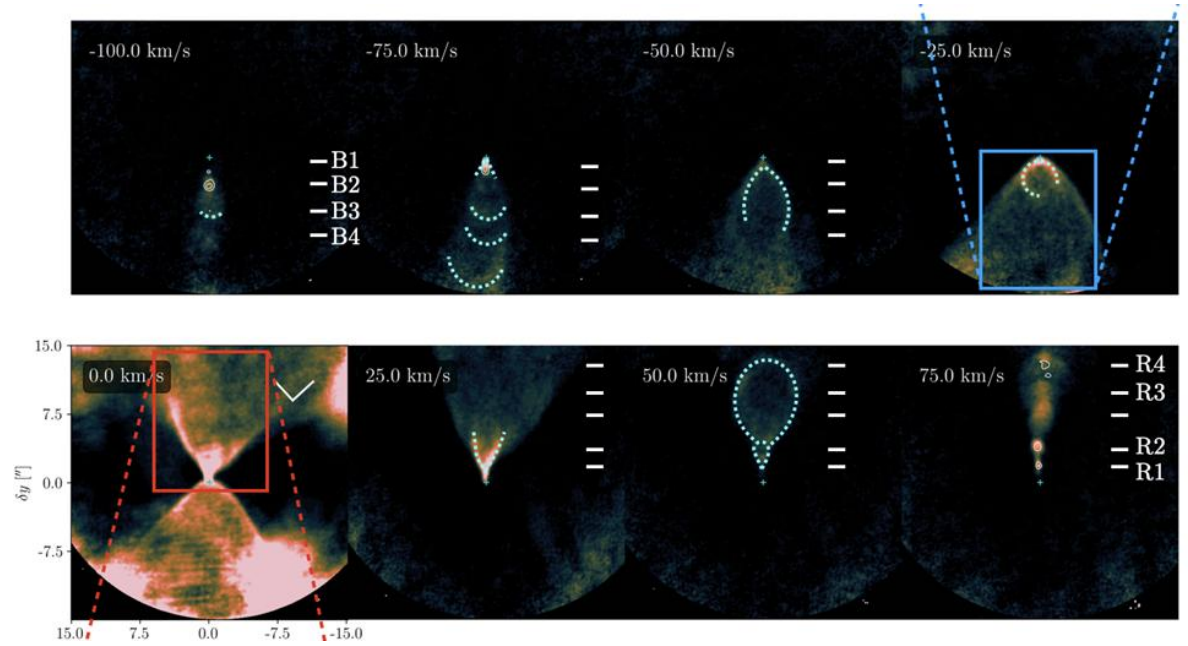

Filament上の構造がノットと中心を結ぶ
SiOは周辺のISMとの相互作用による
reverse shockに伴う？